Tropospheric NO_2 Measurements Using a Three-wavelength Optical Parametric Oscillator Differential Absorption Lidar

Jia Su[1], M. Patrick McCormick[1,*], Matthew S. Johnson[2], John T. Sullivan[3], Michael J. Newchurch[4], Timothy A.Berkoff[5], Shi Kuang[4], Guillaume P. Gronoff[5, 6]

[1]Center for Atmospheric Sciences, Department of Atmospheric and Planetary Sciences, Hampton University, Hampton, Virginia 23668, USA

[2] Earth Science Division, NASA Ames Research Center, Moffett Field, CA, USA

[3]NASA Goddard Space Flight Center, Chemistry and Dynamics Laboratory, Greenbelt, MD 20771, USA

[4]Atmospheric and Earth Science Department, University of Alabama in Huntsville, Huntsville, Alabama, USA

[5]NASA Langley Research Center, Hampton, VA, 23681, USA

[6]Science Systems and Applications, Inc, VA, 23681, USA

Correspondence to: M. Patrick McCormick (PAT.MCCORMICK@HAMPTONU.EDU)

Abstract

The conventional two-wavelength Differential Absorption Lidar (DIAL) has measured air pollutants such as nitrogen dioxide (NO_2). However, high concentrations of aerosol within the planetary boundary layer (PBL) can cause significant retrieval errors using only a two-wavelength DIAL technique to measure NO_2. We proposed a new technique to obtain more accurate measurements of NO_2 using a three-wavelength DIAL technique based on an Optical Parametric Oscillator (OPO) laser. This study derives the three-wavelength DIAL retrieval equations necessary to retrieve vertical profiles of NO_2 in the troposphere. Additionally, two rules to obtain the optimum choice of the three wavelengths applied in the retrieval are designed to help increase the differences of the NO_2 absorption cross sections and reduce aerosol interference. NO_2 retrieval relative uncertainties caused by aerosol extinction, molecular

extinction, absorption of gases other than the gas of interest and backscattering are calculated using two-wavelength DIAL (438 nm and 439.5 nm) and three-wavelength DIAL (438 nm, 439.5 nm and 441 nm) techniques. The retrieval uncertainties of aerosol extinction using the three-wavelength DIAL technique are reduced to less than 2% of using the two-wavelength DIAL technique. Moreover, the retrieval uncertainty analysis indicates that the three-wavelength DIAL technique can reduce more fluctuation caused by aerosol backscattering than two-wavelength DIAL technique. This study presents NO_2 concentration profiles which were obtained using the HU (Hampton University) three-wavelength OPO DIAL. As a first step to assess the accuracy of the HU lidar NO_2 profiles, we compared the NO_2 profiles to simulated data from WRF-Chem model. This comparison suggests that the NO_2 profiles retrieved with the three-wavelength DIAL technique have similar vertical structure, and magnitudes typically within ±0.1 ppb, of modeled profiles.

1. Introduction

Nitrogen dioxide (NO_2) plays a critical role in the tropospheric chemistry and is one of reactive gases collectively referred to as "nitrogen oxides" (NO_x = nitric oxide and nitrogen dioxide (NO + NO_2)) [U.S. EPA, 2018]. The sources of NO_x emissions include transportation (on-road vehicles, airplanes, trains, ships), wood burning, industrial and chemical processes, activities for oil and gas development, soil emissions, lightning and wildfires (see Nitrogen Oxides Emissions indicator) [U.S. EPA, 2018]. Once emitted, NO reacts rapidly in the presence of ozone to form NO_2. In U.S. urban locations, most measured airborne NO_2 comes from the reaction of these two precursors, rather than from direct NO_2 emissions [Bertram, et al., 2005; Beirle, et al., 2011]. Scientific evidence indicates that short-term NO_2 exposure, ranging from 30 minutes to 24 hours, can cause the exacerbation of asthma symptoms, in some cases resulting in hospitalization

[Berglund, et al., 1993]. Long-term NO_2 exposure is likely to have a causal relationship with respiratory effects, based on evidence for the development of asthma [U.S. EPA, 2016]. And NO_2 will be included in future cycles of the Global Burden of Disease as global exposure estimates and evidence on their role as independent risk factors accumulates [Larkin et al., 2017]. Additionally, atmospheric processing of NO_2 leads to the formation of nitrogen-bearing particles that can eventually deposit to the surface, causing acidification, nitrogen enrichment, and other ecological effects [Russell et al., 2012]. Local or global NO_2 monitoring is essential for understanding atmospheric chemistry as well as for human-health and environmental management and control.

Measurements of the intensity of ultraviolet or visible absorption spectra from the ground or from satellites are commonly used to retrieve the column density of NO_2 [Celarier et al., 2008; Valks et al., 2011; Berg et al., 2012]. Satellite-based instruments such as Ozone Monitoring Instrument (OMI), Global Ozone Monitoring Experiment (GOME and GOME-2) and SCanning Imaging Absorption SpectroMeter for Atmospheric CHartographY (SCIAMACHY) can provide global scale NO_2 column measurements during daytime [Boersma et al., 2008; Bucsela et al., 2008]. Moreover, plumes of NO_2 by cities, power plants, and even ships can be tracked using the recent high spatial resolution observations of NO_2 from TROPOMI on Sentinel-5P since 2017 [Lorente, et al., 2019; Georgoulias et al., 2020]. However, they are unable to obtain local high temporal resolution NO_2 emissions such as variations in hourly NO_2 concentrations due to their long repeat cycle, since the lifetime of tropospheric NO_2 is only about 6 hour in summer and 18-24 hours in winter due to photochemical effect [Beirle, et al., 2003; Cui et al., 2016]. In addition, measurements of tropospheric NO_2 from satellite or aircraft are also influenced and limited by clouds [Bovensmann et al., 1999; Liang et al., 2017]. Ground-based measurements of column

NO_2 from instruments such as Pandora using differential optical absorption spectroscopy (DOAS) are often used for the validation of satellite instruments [Herman et al., 2009; Lamsal et al., 2014; Kollonige et al., 2018]. In situ measurements of near-surface NO_2 can best monitor local emissions. However, at this point in time, they cannot provide vertically-resolved measurements. Balloon measurements using a NO_2-sonde can produce vertical profiles, but these measurements are very limited in time and space, especially in the Southern Hemisphere. The primary source of data on the vertical distribution of NO_2 comes from operational sites around the world. However, their operation can be expensive and labor-intensive. [Scott et al., 1999; Herman et al., 2009; Sluis et al., 2010].

The DIAL technique offers the potential for autonomous, 24x7 operation, with improved temporal resolution. Absorption of light by molecules is the basis for DIAL and numerous atmospheric constituents absorbing light. Conventional DIAL operates at two absorbing wavelengths, one stronger than the other indicated by on (λ_{on}) and off (λ_{off}) wavelength of the gaseous absorption feature of interest. Because of different absorption at λ_{on} and λ_{off}, the difference between the backscattered laser signals at the two wavelengths can be used to derive the number density of the absorption gas. Taking the log-ratio of these returns at closely spaced wavelengths removes system parameters and attenuation to and from the target of interest [Rothe et al., 1974; Sullivan et al., 2014]. Thus, this technology provides measurements of the concentration of gas, such as NO_2, O_3, and SO_2 at a particular location and time [Fredriksson et al., 1984; Newchurch et al., 2003; Kuang et al., 2013; Sullivan et al., 2017]. The DIAL technique provides the unique capability of remotely monitoring urban/rural area localized NO_2 concentrations/emissions and profiling their tropospheric vertical NO_2 concentration. However, aerosols are abundant within the PBL and can cause significant retrieval errors in a two-

wavelength DIAL technique to measure NO_2. To better understand this aerosol problem and produce a more accurate NO_2 profile measurement, we described a new technique using a three-wavelength DIAL technique based on the intrinsic capabilities of using a multi-wavelength OPO laser system. HU has incorporated an OPO laser into its lidar system. The OPO laser enables researchers to optimize (tune) wavelength choices for specific measurements [P.Weibring et al., 2003]. The three-wavelength DIAL retrieval equations are derived in this study. Our optimum choices for the three wavelengths to be used for our NO_2 retrievals are designed to help increase the difference in NO_2 absorption cross section, and reduce aerosol influence. NO_2 retrieval relative uncertainties are calculated using the two-wavelength DIAL (438 nm and 439.5 nm) and the three-wavelength DIAL (438 nm, 439.5 nm and 441 nm). Tropospheric NO_2 profiles were obtained by applying the proposed technique to HU OPO DIAL lidar. As a first-order assessment, the HU lidar results were compared with simulated data from the WRF-Chem air quality model.

2. Method

To minimize aerosols-interference on the retrievals of NO_2, a three-wavelength DIAL technique was proposed with $\lambda_1 < \lambda_2 < \lambda_3$. Table 1 shows expressions for the extinction and backscatter of molecules and aerosols for these three wavelengths. In Table 1, β_m and β_a are backscatter from molecules and aerosols for the wavelength of λ_2; α_m and α_a are the extinction of molecules and aerosols for the wavelength of λ_2; e is the aerosol Ångström exponent and assumed to be equal for the three wavelengths because the three wavelengths are very close.

Table 1. Extinction and backscatter of molecule and aerosol for wavelengths of λ_1, λ_2 and λ_3.

wavelength	Molecular backscattering	Aerosol backscattering	Molecular extinction	Aerosol extinction
λ_1	$\left(\frac{\lambda_1}{\lambda_2}\right)^{-4}\beta_m$	$\left(\frac{\lambda_1}{\lambda_2}\right)^{-e}\beta_a$	$\left(\frac{\lambda_1}{\lambda_2}\right)^{-4}\alpha_m$	$\left(\frac{\lambda_1}{\lambda_2}\right)^{-e}\alpha_a$
λ_2	β_m	β_a	α_m	α_a

λ_3	$\left(\frac{\lambda_3}{\lambda_2}\right)^{-4}\beta_m$	$\left(\frac{\lambda_3}{\lambda_2}\right)^{-e}\beta_a$	$\left(\frac{\lambda_3}{\lambda_2}\right)^{-4}\alpha_m$	$\left(\frac{\lambda_3}{\lambda_2}\right)^{-e}\alpha_a$

The three elastic lidar equations can be expressed as:

$$X(\lambda_1,Z)=C_1\frac{\left[\left(\frac{\lambda_1}{\lambda_2}\right)^{-4}\beta_m(Z)+\left(\frac{\lambda_2}{\lambda_1}\right)^{-e}\beta_a(Z)\right]}{Z^2}\exp\left\{-2\int_0^Z\left[\left(\frac{\lambda_1}{\lambda_2}\right)^{-4}\alpha_m(z)+\left(\frac{\lambda_2}{\lambda_1}\right)^{-e}\alpha_a(z)+\sigma_N(\lambda_1,z)N_N(z)+O_{abs}(\lambda_1,z)\right]dz\right\} \quad (1)$$

$$X(\lambda_2,Z)=C_2\frac{[\beta_m(Z)+\beta_a(Z)]}{Z^2}\exp\{-2\int_0^Z[\alpha_m(z)+\alpha_a(z)+\sigma_N(\lambda_2,z)N_N(z)+O_{abs}(\lambda_2,z)]dz\} \quad (2)$$

$$X(\lambda_3,Z)=C_3\frac{\left[\left(\frac{\lambda_3}{\lambda_2}\right)^{-4}\beta_m(Z)+\left(\frac{\lambda_3}{\lambda_2}\right)^{-e}\beta_a(Z)\right]}{Z^2}\exp\{-2\int_0^Z[\left(\frac{\lambda_3}{\lambda_2}\right)^{-4}\alpha_m(z)+\left(\frac{\lambda_3}{\lambda_2}\right)^{-e}\alpha_a(z)+\sigma_N(\lambda_3,z)N_N(z)+O_{abs}(\lambda_3,z)dz\} \quad (3)$$

where X is the lidar signal; C_1, C_2 and C_3 are lidar constants; the subscripts *a* and *m* represent aerosol, and molecule, respectively; σ_N is the absorption cross section for the gas of interest; N_N is the molecular density of the gas of interest; O_{abs} is absorption of gases other than the gas of interest and z is the altitude. The molecular density of the gas of interest can be obtained using Eq. (1), (2) and (3).

NO_2 density retrieval equation can be expressed as:

$$N_N(Z)=\frac{\frac{1}{2}\times\frac{d}{dz}\left[ln\frac{X(\lambda_1,Z)X(\lambda_3,Z)}{X(\lambda_2,Z)^2}\right]-AED(z)-MED(z)-OAD(z)-B(z)}{\Delta\sigma_N} \quad (4)$$

$$\Delta\sigma_N=2\sigma_N(\lambda_2)-\sigma_N(\lambda_1)-\sigma_N(\lambda_3) \quad (5)$$

$$B(z)=\frac{1}{2}\frac{d}{dz}\left[ln\frac{\left[\left(\frac{\lambda_3}{\lambda_2}\right)^{-4}\beta_m(Z)+\left(\frac{\lambda_3}{\lambda_2}\right)^{-e}\beta_a(Z)\right]\left[\left(\frac{\lambda_1}{\lambda_2}\right)^{-4}\beta_m(Z)+\left(\frac{\lambda_1}{\lambda_2}\right)^{-e}\beta_a(Z)\right]}{[\beta_m(Z)+\beta_a(Z)]^2}\right] \quad (6)$$

$$AED(z)=K\alpha_a(Z) \qquad K=2-\left(\frac{\lambda_1}{\lambda_2}\right)^{-e}-\left(\frac{\lambda_3}{\lambda_2}\right)^{-e} \quad (7)$$

$$MED(z)=\left[2-\left(\frac{\lambda_1}{\lambda_2}\right)^{-4}-\left(\frac{\lambda_3}{\lambda_2}\right)^{-4}\right]\alpha_m(Z) \quad (8)$$

$$OAD(z)=2O_{abs}(\lambda_2,z)-O_{abs}(\lambda_1,z)-O_{abs}(\lambda_3,z) \quad (9)$$

where AED, MED, OAD and B are the correction terms of aerosol extinction, molecular extinction, absorption of gases other than the gas of interest and backscattering, respectively. Because the atmospheric molecular density is relatively stable, MED can be corrected using a numerical model or local real-time radiosonde data. OAD can be removed by choosing

appropriate wavelengths. However, aerosol is variable especially in PBL. For correction of AED and B, we need accurate aerosol measurements. However, accurate aerosol measurements are not easily to be obtained. From the above NO_2 retrieval relative equation, all of correction terms are related to the three wavelengths, so how to choose the three wavelengths is very critical to reduce correction terms and improve the accuracy of NO_2 retrievals. We designed two rules to obtain the optimum choice for the three wavelengths:

a. The chosen three wavelengths increase differences of the NO_2 absorption cross section ($\Delta\sigma_N$) to improve NO_2 retrieval.

According to Eq. (4), the more $\Delta\sigma_N$ is, the less all of correction terms are. So the chosen three wavelengths should help to increase $\Delta\sigma_N$. Generally, researchers only used an increasing absorption method ($\sigma_N(\lambda_1)<\sigma_N(\lambda_2)<\sigma_N(\lambda_3)$) or a decreasing absorption method ($\sigma_N(\lambda_1)>\sigma_N(\lambda_2)>\sigma_N(\lambda_3)$) (illustrated in Fig. 1) to choose the three wavelengths [Wang, et al., 1997; Liu, et al., 2017]. Wang used three wavelengths corresponding to the strong, medium and weak absorption of O_3 to obtain an accurate stratospheric ozone profile in the presence of volcanic aerosols. Liu used three wavelengths of 448.10nm, 447.20nm and 446.60 nm corresponding to the strong, medium and weak absorption of NO_2 to retrieve NO_2. Equation (10) and (11) are calculated values of $\Delta\sigma_N$ for the increasing absorption method and the decreasing absorption method using Eq. (5). Using the increasing absorption method and the decreasing absorption method to choose the three wavelengths, the values of $\Delta\sigma_N$ are both decreased according to Eq. (10) and (11) compared to the conventional two-wavelength DIAL technique. According to characteristics of the NO_2 absorption spectrum showed in Fig. 2, a bumping absorption method ($\sigma_N(\lambda_1)<\sigma_N(\lambda_2)\&\sigma_N(\lambda_3)<\sigma_N(\lambda_2)$) is designed to choose the three wavelengths which can increase value of $\Delta\sigma_N$ compared to the two-wavelength DIAL technique according to Eq. (12).

However, for DIAL systems to measure other atmospheric gases like ozone, it is only practical to use wavelength selection Method B because of the shape of the ozone absorption spectrum (lacking narrow peaks).

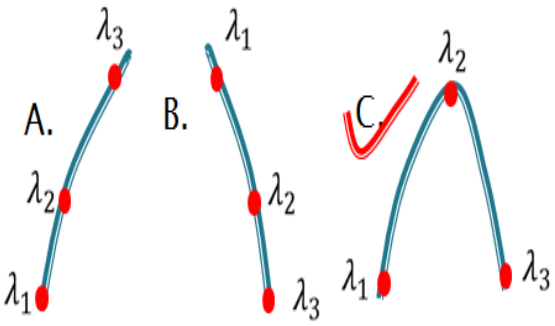

Fig.1 The three-wavelength chosen methods: Increasing absorption method (A), Decreasing absorption method (B) and Bumping absorption method (C)

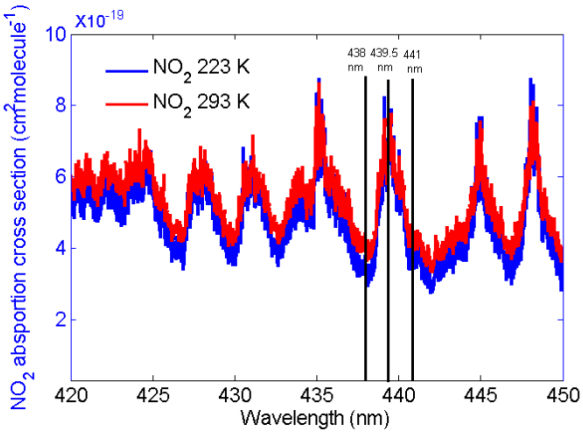

Fig.2 NO_2 strong absorption cross section between 420 nm and 450 nm

Increasing absorption method: $\Delta\sigma_N = abs[\sigma_N(\lambda_2) - \sigma_N(\lambda_1)] - abs[\sigma_N(\lambda_2) - \sigma_N(\lambda_3)]$ (10)

Decreasing absorption method: $\Delta\sigma_N = abs[\sigma_N(\lambda_2) - \sigma_N(\lambda_3)] - abs[\sigma_N(\lambda_2) - \sigma_N(\lambda_1)]$ (11)

Bumping absorption method: $\Delta\sigma_N = abs[\sigma_N(\lambda_2) - \sigma_N(\lambda_1)] + abs[\sigma_N(\lambda_2) - \sigma_N(\lambda_3)]$ (12)

b. The chosen three wavelengths can reduce or remove AED.

It means the value of AED is equal or close to 0. Choosing the appropriate three wavelengths to make the value of K in Eq. (12) equal or close to 0, the value of AED will be equal or close to 0. The value of K in Eq. (12) changes with different aerosol Ångström exponents. For example, to remove boundary layer aerosol influence, we can set aerosol Ångström exponents=1 to calculate

the value of K to choose the three wavelengths because the size of aerosol in the boundary layer is typically large [Schuster, et al., 2006].

3. HU three-wavelength OPO DIAL system

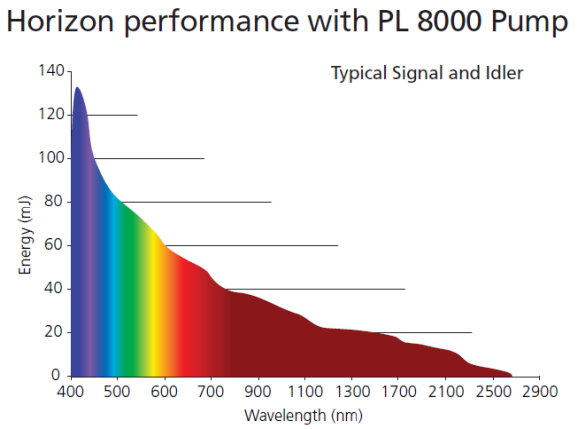

Description	
Pulsewidth (nsec)	3-7
Pointing Stability (urad)	<±100
Linewidth (cm^{-1})	
Unseeded	3-7
Doubling/Mixing	<10
Energy Stability (%,99% of shots)	<±10
Divergence (mrad,FWHM)	<2 (both axes)
Beam Diameter (mm, near field)	4-7
Beam Roundness (%, near field)	>85
Polarization (%)	
Signal Horizontal	>99
Idle Horizontal	>99

Fig.3 Continuum Horizon II energy outputs (a) and parameters (b) with PL 8000 pump

The HU lidar is located on the campus of HU (37.02° N, 76.34° W) in Hampton, VA. A Continuum Horizon II tunable OPO laser and a Continuum Powerlite DLS 8000 pump laser have recently been incorporated into HU lidar system. The OPO laser enables researchers to optimize (tune) the wavelength choices and provides more flexibility than fixed-frequency wavelength shifters such as Raman cells. The wavelength tuning range of our OPO extends from 192 nm to 2750 nm. This range is fully automated with precision scanning for true hands-free operation. Fig. 3(a) and (b) show the Continuum Horizon II output energy and its parameters. The OPO laser energy outputs between 400 nm and 500 nm which overlap with the NO_2 strong absorption spectral zone in Fig. 2 produce near the maximum possible power in the spectrum. Combining the OPO laser energy outputs, NO_2 absorption spectral and two three-wavelength chosen rules, 438 nm, 439.5 nm and 441 nm shown in Fig. 2 result in the wavelengths of HU three-wavelength DIAL system because $\Delta\sigma_N$ of the three-wavelength pair is more than other three-wavelength

pairs in NO_2 strong absorption spectral zone and the *K* value of the three-wavelength is 0.000023 (close to 0). The HU lidar system currently consists of a Continuum OPO laser system as the light source, a 48-inch non-coaxial Cassegrainian-configured telescope receiver, a light separation system that uses beam splitters and interference filters, a detecting system including photomultiplier tubes (PMT) and avalanche photodiodes (APDs) and a Licel optical transient recorder. A schematic of the lidar system is shown in Fig.4. The system can be configured to measure multi-wavelength aerosols and NO_2 density. High-resolution backscatter measurements extend from the boundary layer (1.2 km) to free troposphere. The pump laser operates at three fixed wavelengths (1064, 532, and 354.7 nm). The 354.7-nm laser is mostly reflected into OPO laser to produce three-wavelength (338 nm, 339.5 nm and 441 nm). Steering mirrors whose axes are aligned with a receiving telescope axis directs these laser outputs into the atmosphere. The laser backscatter is collected by a 48-inch diameter telescope and split into specific wavelength bands by a beam separation unit, which combines filters and beam-splitters for dispersion of the return backscatter to various detection channels. Using filters and beam-splitters makes the beam-splitting system simple, compact, and easy to change or add other spectral channels for other measurements. Currently, wavelengths of 438 nm, 439.5 nm, 441 nm, 354.7 nm, 532 nm and 1064 nm are focused to PMTs and APD, and recorded by a Licel data-collecting system for measurements of aerosol, and NO_2.

To demonstrate that the HU three-wavelength OPO DIAL system can effectively reduce aerosol influence and accurately retrieve NO_2, retrieval correction terms of AED, MED, OAD and B in Eq. (4) are simulated using two-wavelength DIAL technique (438 nm and 439.5 nm) and the three-wavelength DIAL technique (438 nm, 439.5 nm and 441 nm). Ozone was used for the simulation of OAD because only ozone absorption can produce a little influence on NO_2 retrieval

based on HITRAN 1.1.2.0 database. Atmospheric data of aerosol, molecule, O_3 and NO_2 for these simulations are from the HU local lidar aerosol measurements, radiosonde, NASA Tropospheric Ozone Lidar Network (TOLNet) and NASA Deriving Information on Surface Conditions from COlumn and VERtically Resolved Observations Relevant to Air Quality (DISCOVER-AQ) measurements shown in Fig.5. Extinction and backscatter of aerosol at 438 nm, 439.5 nm and 441 nm can be calculated from aerosol extinction profile at 532 nm in Fig.5 (a) with the setting of lidar ratio=50 and *e*=1, 2 and 3. Lidar ratio is wavelength dependent and its value in the visible band is in general smaller than in the UV band for the same type of aerosols [Kuang et al., 2020; Reid et al., 2017]. Absorption of NO_2 and O_3 at 438 nm, 439.5 nm and 441 nm can be calculated using their mixing ratio profiles in Fig.5 (b) and their absorption cross-sections from HITRAN 1.1.2.0 database. MED, AED, OAD, B and absorption difference of NO_2 (NAD) are simulated using two-wavelength DIAL technique with different aerosol Ångström exponents (*e*=1, 2 and 3) shown in Fig. 6 (a), (c) and (e), and the three-wavelength DIAL technique shown in Fig.6 (b), (d) and (f). In Fig. 6, red lines are NAD; black lines are MED; deep blue lines are AED; light blue lines are OAD. In Fig. 6, all OAD is far less than NAD. It is concluded that ozone absorption has negligible influence on the retrieval of NO_2. In Fig. 6 (a), (c) and (d), MED and AED in PBL are both more than NAD using the two-wavelength DIAL technique. Because atmospheric molecules are relatively stable, MED can be corrected using local model or real-time radiosonde data. However, aerosol is variable, so aerosols are a significant uncertainty for retrieving NO_2 with the conventional two-wavelength DIAL technique. In Fig. 6 (b), (d) and (f), MED and AED in boundary layer are both much smaller than NAD using proposed three-wavelength DIAL technique. It is proven that three-wavelength DIAL technique can effectively decrease retrieval errors caused by aerosol extinction. From Fig.5, we

can see AED using three-wavelength DIAL technique can be reduced to less than 2% of AED using two-wavelength DIAL technique at least. Therefore, even if AED is not corrected, NO_2 still can be accurately retrieved. Moreover, simulated B using the two-wavelength DIAL technique and the three-wavelength DIAL technique are shown in Fig. 6 with green lines. The sharp change on vertical adjacent aerosol backscatter can cause drastic changes of B term. In Fig. 6, the value of B term using three-wavelength DIAL technique is far less than using two-wavelength DIAL technique. So the three-wavelength DIAL technique can reduce more fluctuation caused by aerosol backscattering than two-wavelength DIAL technique.

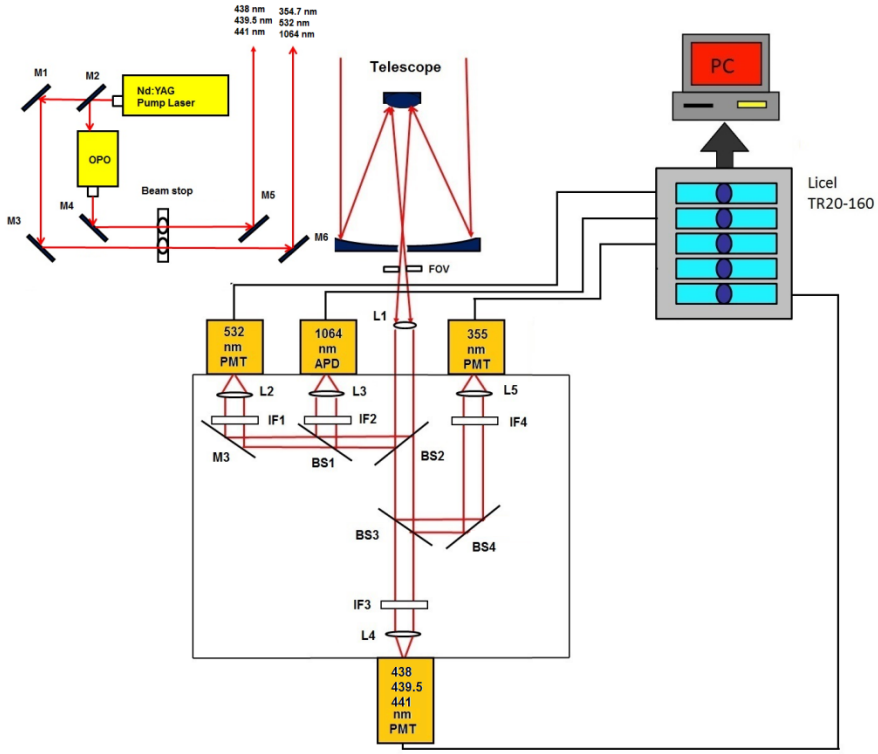

Fig.4 HU lidar system (L-lens, M-mirror, BS-beam-splitter, IF-interference filter, FOV-field of view, PMT-Photomultiplier tube, APD-Avalanche Photodetector)

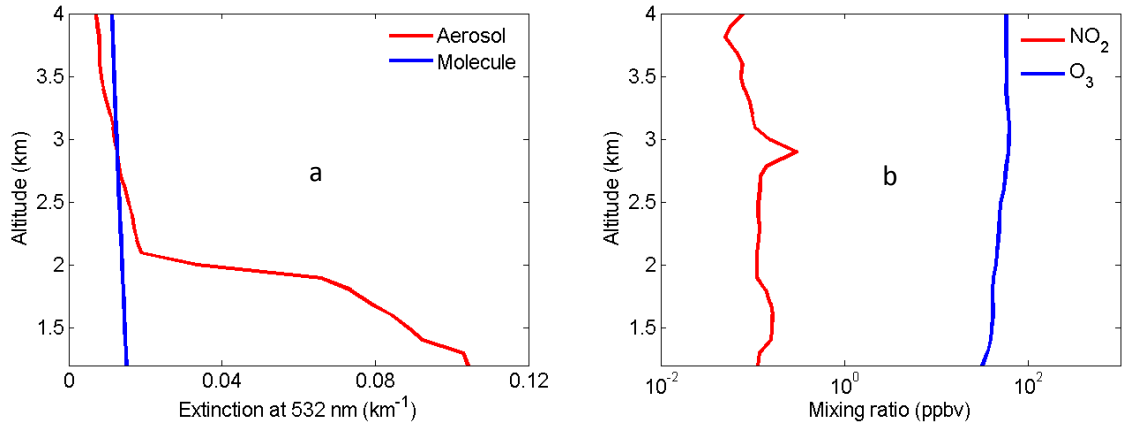

Fig.5 Atmospheric profiles used for modeling NO_2 lidar correction terms. (a) Aerosol extinction profile (red) at 532 nm measured by the HU lidar and molecular extinction profile (blue) at 532 nm derived from local radiosonde data; (b) NO_2 (red) and O_3 (blue) mixing ratio profiles from NASA DISCOVER-AQ and TOLNet.

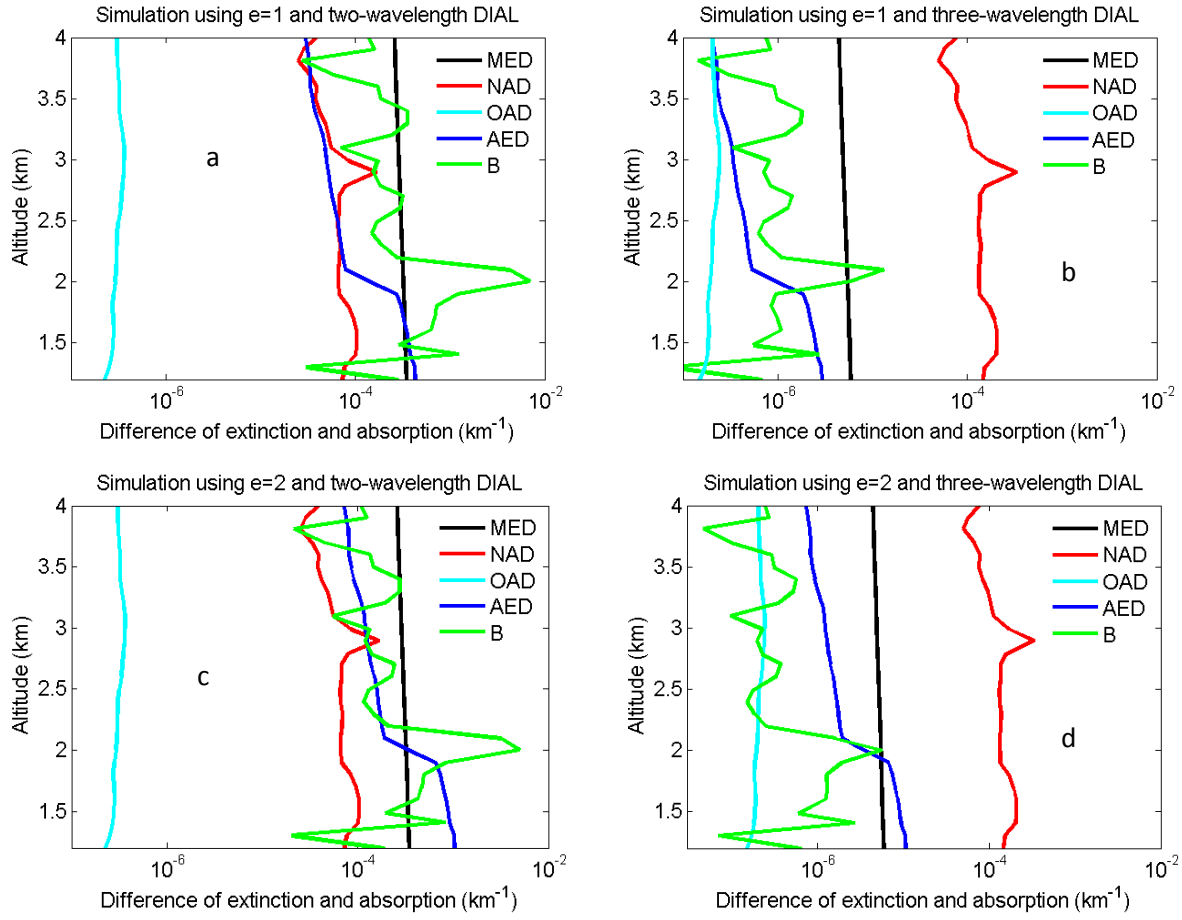

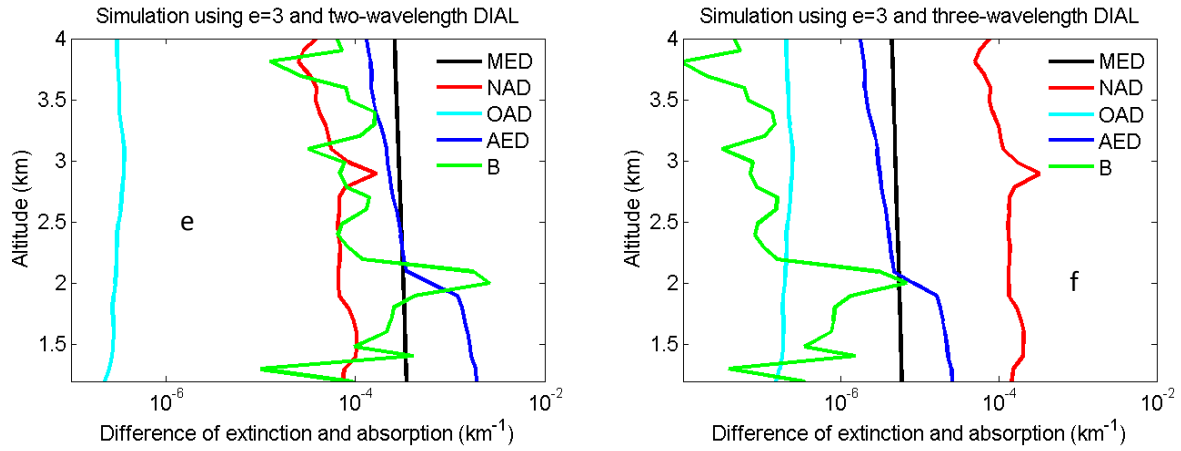

Fig.6 Simulated MED (black), NAD (red), OAD (light blue), AED (deep blue)and B (green) using two-wavelength DIAL with e=1(a), e=2 (c) and e=3 (e) and three-wavelength DIAL technique with e=1(b), e=2(d) and e=3(f).

4. Uncertainty analysis

According to NO_2 retrieval Eq.4, the NO_2 measurement uncertainty is due to molecule, absorption of gases other than the gas of interest, aerosol and noise of lidar signals. The total relative uncertainty can be expressed as Eq. (13) [Leblanc et al., 2016].

$$U_{NO_2}(z) = \sqrt{U_{AED}(z)^2 + U_{MED}(z)^2 + U_{OAD}(z)^2 + U_B(z)^2 + U_S(z)^2} \quad (13)$$

$$U_{MED}(z) = \frac{u[MED(z)]}{N_N(z)\Delta\sigma_N} = \frac{\left[2-\left(\frac{\lambda_2}{\lambda_1}\right)^4-\left(\frac{\lambda_2}{\lambda_3}\right)^4\right]u[\alpha_m(z)]}{N_N(Z)\Delta\sigma_N} = \frac{\left[2-\left(\frac{\lambda_2}{\lambda_1}\right)^4-\left(\frac{\lambda_2}{\lambda_3}\right)^4\right]\sigma_m u[N_m(z)]}{N_N(Z)\Delta\sigma_N} \quad (14)$$

$$U_{OAD}(z) = \frac{u[OAD(z)]}{N_N(Z)\Delta\sigma_N} = \frac{u[2O_{abs}(\lambda_2,z)-O_{abs}(\lambda_1,z)-O_{abs}(\lambda_3,z)]}{N_N(Z)\Delta\sigma_N} = \frac{[2\sigma_o(\lambda_2,z)-\sigma_o(\lambda_1,z)-\sigma_o(\lambda_3,z)]u[N_o(z)]}{N_N(Z)\Delta\sigma_N} \quad (15)$$

$$U_{AED}(z) = \frac{u[AED(z)]}{N_N(Z)\Delta\sigma_N} = \frac{\left[2-\left(\frac{\lambda_2}{\lambda_1}\right)^e-\left(\frac{\lambda_2}{\lambda_3}\right)^e\right]u[\alpha_a(z,s)]}{N_N(Z)\Delta\sigma_N} \quad (16)$$

$$U_B(z) = \frac{u\left\{\frac{1}{2}\frac{d}{dz}\left[ln\frac{\left[\left(\frac{\lambda_2}{\lambda_3}\right)^4\beta_m(z)+\left(\frac{\lambda_2}{\lambda_3}\right)^e\beta_a(z,s)\right]\left[\left(\frac{\lambda_2}{\lambda_1}\right)^4\beta_m(Z)+\left(\frac{\lambda_2}{\lambda_1}\right)^e\beta_a(z,s)\right]}{[\beta_m(Z)+\beta_a(Z,s)]^2}\right]\right\}}{N_N(Z)\Delta\sigma_N} \quad (17)$$

$$U_S(z) = \frac{u\left\{\frac{1}{2}\times\frac{d}{dz}\left[ln\frac{X(\lambda_1,Z)(\lambda_3,Z)}{X(\lambda_2,Z)^2}\right]\right\}}{N_N(Z)\Delta\sigma_N} =$$

$$\frac{\frac{1}{2}\times\sqrt{\left\{\frac{d\left\{\frac{d}{dz}\left[ln\frac{X(\lambda_1,Z)(\lambda_3,Z)}{X(\lambda_2,Z)^2}\right]\right\}}{d[X(\lambda_1,Z)]}\times u[X(\lambda_1,Z)]\right\}^2+\left\{\frac{d\left\{\frac{d}{dz}\left[ln\frac{X(\lambda_1,Z)(\lambda_3,Z)}{X(\lambda_2,Z)^2}\right]\right\}}{d[X(\lambda_2,Z)]}\times u[X(\lambda_2,Z)]\right\}^2+\left\{\frac{d\left\{\frac{d}{dz}\left[ln\frac{X(\lambda_1,Z)(\lambda_3,Z)}{X(\lambda_2,Z)^2}\right]\right\}}{d[X(\lambda_3,Z)]}\times u[X(\lambda_3,Z)]\right\}^2}}{N_N(Z)\Delta\sigma_N} \quad (18)$$

where U_{NO2} is NO_2 total retrieval relative uncertainty using three-wavelength DIAL technique; U_{MED}, U_{OAD}, U_{AED}, U_B and U_s are NO_2 retrieval relative uncertainty caused by molecule, absorption of gases other than the gas of interest, aerosol (extinction and backscattering) and noise of lidar signals expressed as Eq. (14), (15), (16), (17) and (18); u is uncertainty function; N_m and N_o are number density (ND) of air and ozone; σ_m is Rayleigh scattering cross section; σ_o is absorption cross section of ozone; S is lidar ratio.

From Eq. (14) and (15), U_{MED} and U_{OAD} are determined by $u[N_m(z)]$ and $u[N_o(z)]$ (uncertainties of N_m and N_o). In our measurements, profiles of temperature and pressure from local radiosonde are used to calculate N_m. Usually, one radiosonde is launched for about 8-hour measurement. One profile of air number density from local radiosonde is used to correct 8-hour NO_2 measurements. According to statistics of 8-hour variation of temperature and pressure in local four seasons, the uncertainty of N_m is between 1% and 3%. U_{MED} using two-wavelength DIAL technique and the three-wavelength DIAL technique are calculated according to Eq. (14) with the uncertainty of N_a as 1%, 2% and 3% shown in Fig. 7(a). U_{MED} using three-wavelength DIAL technique is far less than using two-wavelength DIAL technique. N_o is obtained from local measurements. Because of very low values of ozone absorption cross section differentials, with the uncertainty of N_o as 50% and 100%, U_{OAD} using two-wavelength DIAL technique and using the three-wavelength DIAL technique are both less 0.5% from Fig.7 (b). Ozone absorption correction is neglect in NO_2 retrieval. From Eq. (16) and (17), U_{AED} and U_B are determined by

uncertainties of a_a, β_a and e. For HU lidar system, 532-nm elastic signals are used to calculate a_a and β_a with Fernald method to correct NO_2 retrieval [Fernald et al., 1972]. 50 sr is usually chosen as lidar ratio to retrieve a_a and β_a. The lidar ratio is variable, so uncertainties of a_a and β_a are caused by chosen lidar ratio. The range of lidar ratio is about from 30 sr to 70 sr for 532 nm. The uncertainty of lidar ratio is 40% for 50 sr. The uncertainties of a_a and β_a are calculated with uncertainty of lidar ratio as 40%. Finally, U_{AED} and U_B using two-wavelength DIAL technique and using the three-wavelength DIAL technique are calculated with the Ångström exponent as 1, 2 and 3 shown in Fig. 8, 9 and 10. From these figures, U_{AED} and U_B using three-wavelength DIAL technique are both less 4%. However, U_{AED} below 2 km using two-wavelength DIAL technique are more than 90% after correction of aerosol extinction. From Eq. (18), U_s is determined by uncertainties of three-wavelength lidar signals. The uncertainties of lidar signals with average integration time of 1 minute and 2 minutes are derived from Poisson statistics associated with the probability of detection of a repeated random event [Measures, 1984; Leblanc et al., 2016]. NO_2 number density relative uncertainty owing to the noise of lidar signals with average integration time of 1 minute and 2 minutes are obtained shown in Fig11. We can see U_s using two-wavelength DIAL technique is smaller than using three-wavelength DIAL technique. With increase of average integration time from 1 minute to 2 minutes, U_s can be effectively reduced. At last, U_{NO_2} (the total relative uncertainties of NO_2) with e as 1, 2 and 3 are calculated shown in Fig. 12(a), (b) and (c).

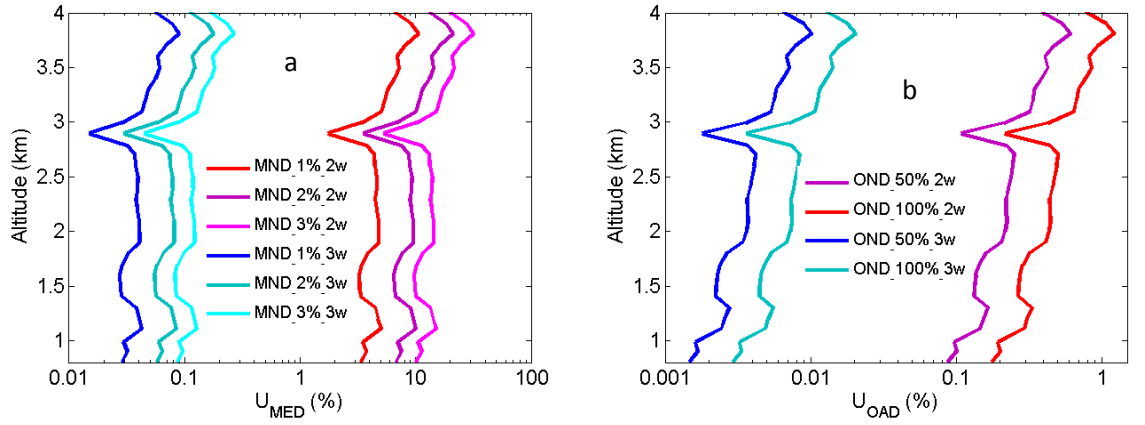

312

313 Fig.7 NO_2 number density relative uncertainty owing to air number density (a) and ozone number density
314 (b).

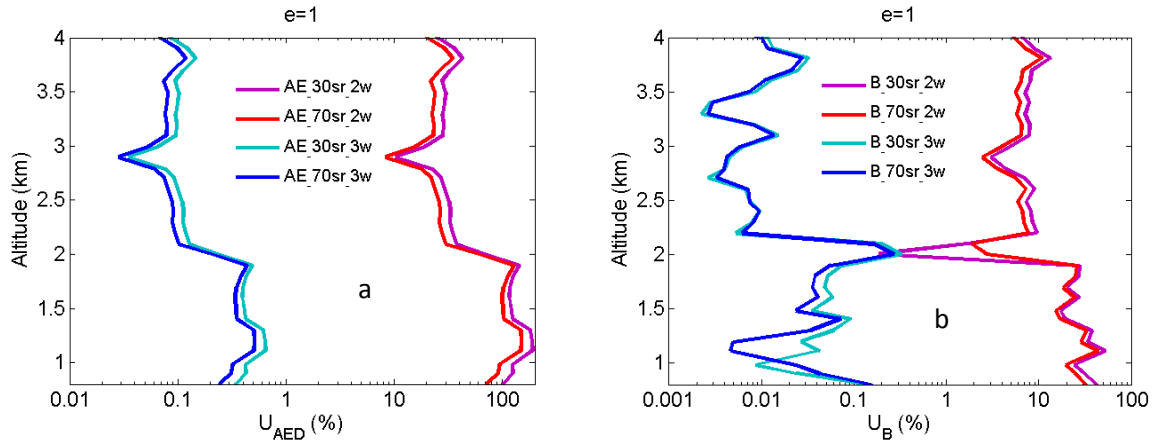

315

316 Fig.8 NO_2 number density relative uncertainty owing to aerosol extinction (a) and backscatter (b) with e=
317 1.

318

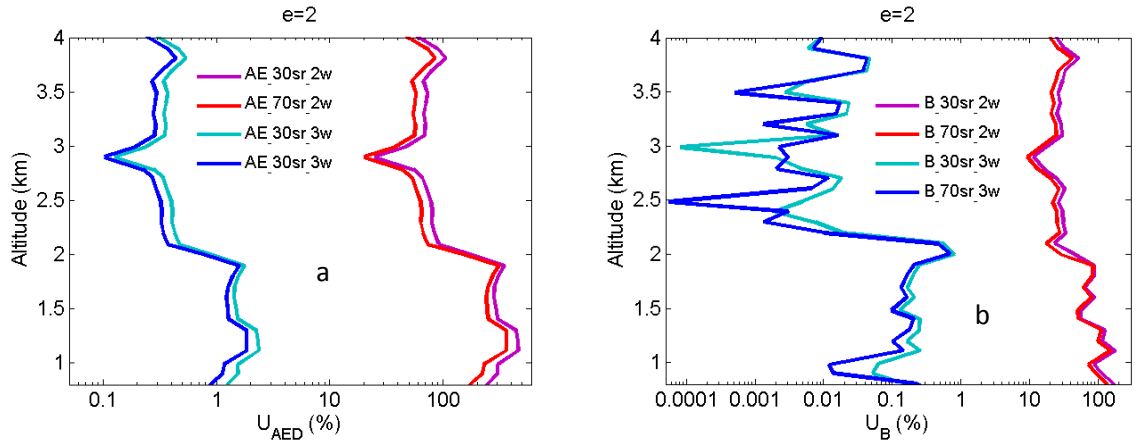

319

320 Fig.9 NO_2 number density relative uncertainty owing to aerosol extinction (a) and backscatter (b) with e=
321 2.

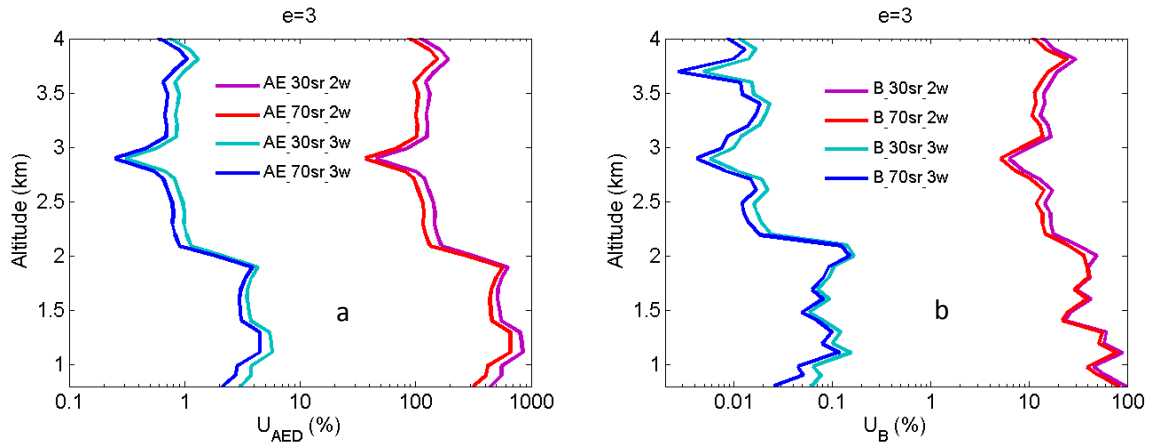

322

323 Fig.10 NO_2 number density relative uncertainty owing to aerosol extinction (a) and backscatter (b) with
324 e=3.

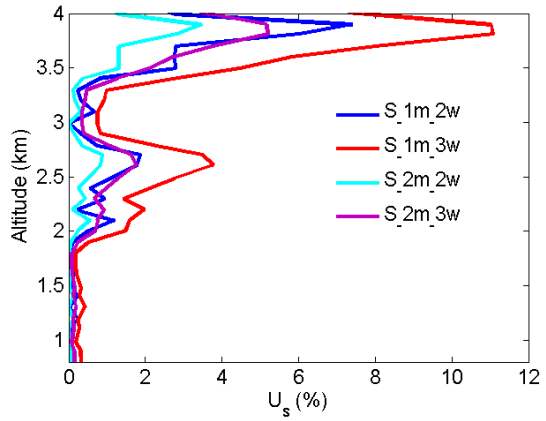

325

326 Fig.11 NO_2 number density relative uncertainty owing to the noise of signals with average of 1 minute
327 and 2 minutes.

328

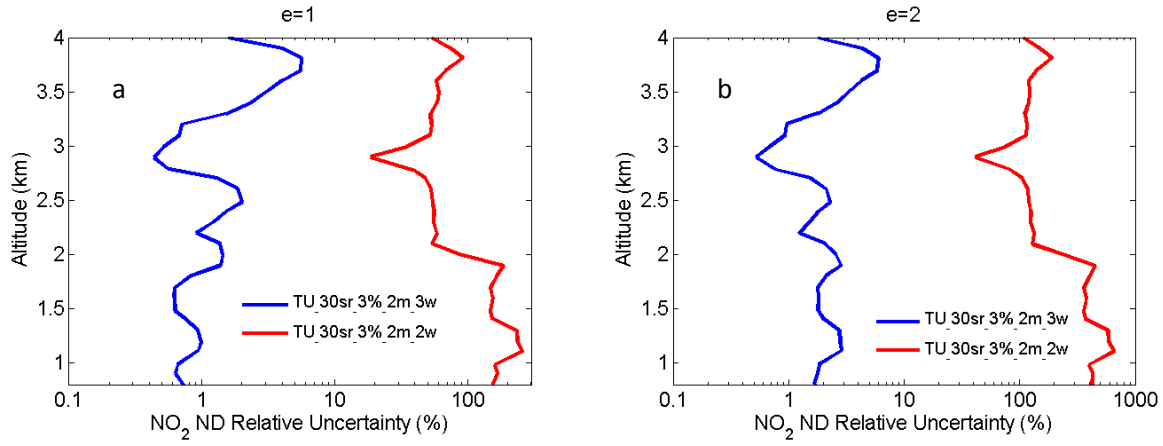

329

330

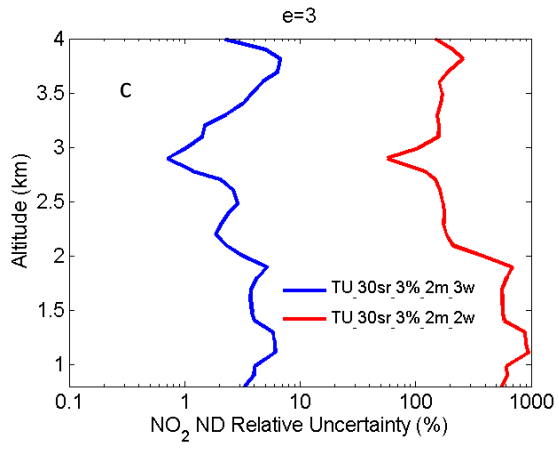

Fig.12 NO_2 number density total relative uncertainty with e=1 (a), e=2 (b) and e=3 (c).

5. Results

The three-wavelength DIAL technique was implemented by the HU lidar measurements during two cases at night and the resulting vertical profiles are presented in Fig. 13. All NO_2 lidar measurements presented here are obtained at times with less than 10% cloud coverage below 8 km. HU lidar 438 nm (blue line), 439.5 nm (red line) and 441 nm (black line) elastic signals measured at 21:00 (local time) on May 13, 2020 and 22:00 (local time) on July 27, 2020 are shown in Fig. 13 (a) and (c), respectively. The average integration time for these signals is 2 minutes. Determined from the lidar elastic signals in Fig. 13 (a) and (c), there is an existing aerosol layer between 2.2 km and 3.5 km on May 13, while July 27 presented a clean atmosphere. Fig. 13 (b) and (d) show retrieved NO_2 profiles using the three-wavelength DIAL technique (red line). The black error bars in Fig.13 (b) and (d) indicate the uncertainty of NO_2 retrieval calculated using Eq. (13). In Fig. 13 (b), the retrieved NO_2 profile between 2.2 km and 3.5 km on May 13 is smooth and not affected by the aerosol layer. The NO_2 profiles (sky-blue line and purple line) were also retrieved using the conventional two-wavelength DIAL technique without and with aerosol correction shown in Fig. 13 (b) resulting in a bump between 2.2 km and 3.5 km in the NO_2 profile retrieved using the two-wavelength DIAL technique. This inconsistency

suggests that the two-wavelength DIAL technique cannot remove AED of the aerosol layer between 2.2 km and 3.5 km and the retrieved NO_2 profile contains AED interference. Moreover, the NO_2 retrievals below 2 km using two-wavelength DIAL technique shown in Fig. 13 (b) and (d) are more than the three-wavelength DIAL technique suggesting that the AED of boundary aerosol was not correctly removed. Aerosol correction is very important for NO_2 retrieval using the conventional two-wavelength DIAL technique [Sasano et al., 1985]. These results suggest that the proposed three-wavelength DIAL technique can effectively remove influence of aerosol on the retrieval of NO_2. As a first-order assessment of the HU lidar NO_2 profiles, we compare the retrieval results to simulated data from the Weather Research and Forecasting Chemistry (WRF-Chem) model (Grell et al., 2005) at 12 km × 12 km spatial resolution and 200 m vertical resolution. Past studies have demonstrated that WRF-Chem simulated NO_2 results show good agreement between the OMI satellite measurements and aircraft measurements [Amnuaylojaroen et al., 2019; Barten et al., 2020] providing a data source to examine the accuracy of the HU retrievals using both two-wavelength DIAL technique and three-wavelength DIAL technique. The HU local NO_2 profiles for these two cases are simulated using WRF-Chem model and shown in Fig. 13 (b) and (d). WRF-Chem simulated NO_2 magnitudes tend to be lower compared to HU retrieved NO_2 profiles using three-wavelength DIAL technique (typically within ±0.1 ppb), except above 3.5 km on May 13, 2020, however, the comparison demonstrates a consistent vertical profile shape between observations and the model simulation. And retrieval results using the three-wavelength DIAL technique are much closer to simulated values compared to using the two-wavelength DIAL technique. These figures also demonstrate that the reduced fluctuations caused by aerosol backscatter when using the three-wavelength DIAL technique results in vertical profiles of NO_2 which are much more consistent with simulated data when compared to

results of the two-wavelength DIAL retrievals. Both the WRF-Chem simulated profiles and the HU retrievals of NO_2 using three-wavelength DIAL technique are associated with uncertainties which could result in the differences in magnitude; however, given the consistent nature in the vertical profile shapes from both data sources provides confidence that the HU lidar is retrieving NO_2 vertical profiles using three-wavelength DIAL technique in the troposphere.

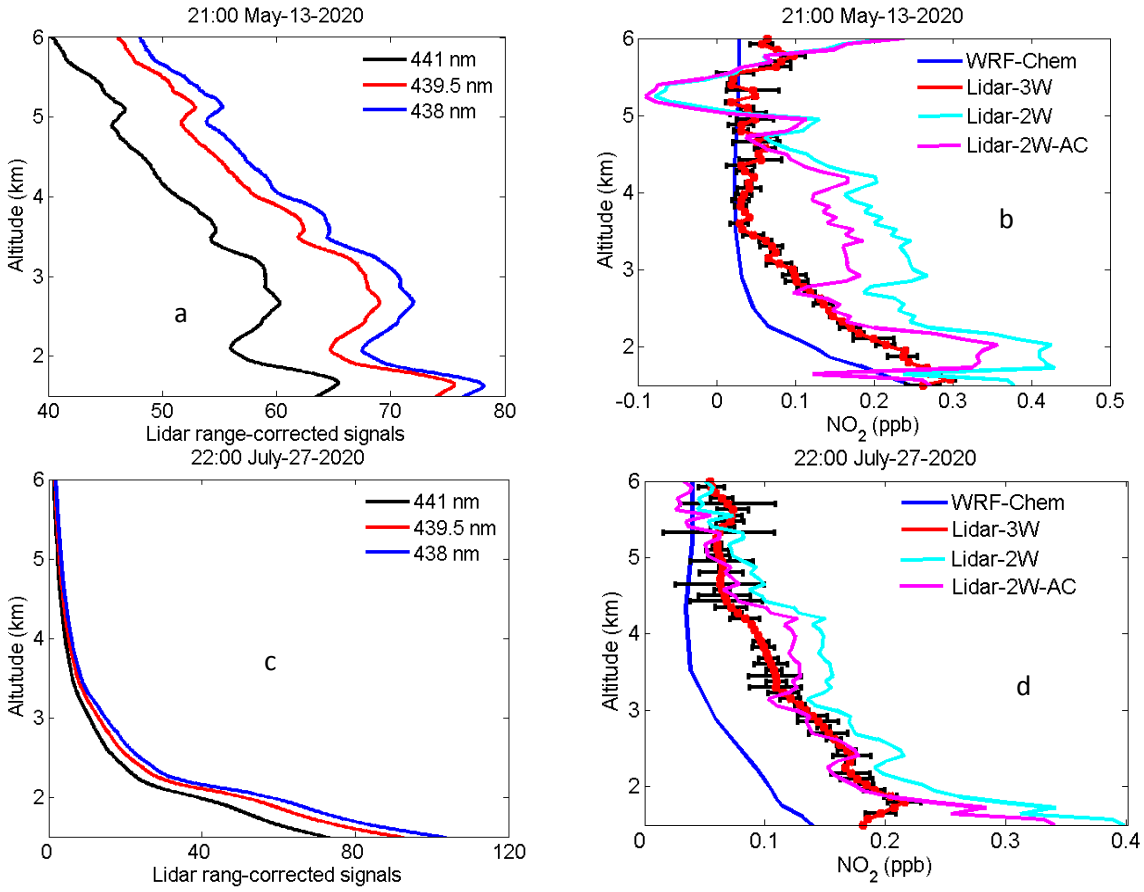

Fig.13 HU lidar 438 nm, 439.5 nm and 441 nm elastic signals measured at 21:00 (local time) on May 13, 2020 (a) and 22:00 (local time) on July 27, 2020 (c); NO_2 profiles obtained using three-wavelength DIAL technique, two-wavelength DIAL technique and WRF-Chem model at 21:00 on May 13, 2020 (b) and 22:00 on July 27, 2020 (d).

6. Conclusion

This study describes a lidar retrieval technique using three wavelengths simultaneously emitted from an OPO laser to measure tropospheric NO_2 profiles. The three-wavelength DIAL retrieval

equations describe how the retrievals decrease errors caused by aerosol interference. Aerosol extinction differences using this proposed technique can be decreased to less than 2% of aerosol extinction differences resulting from a conventional two-wavelength DIAL technique. Comparing the HU lidar results to WRF-Chem model output demonstrates that the NO_2 magnitudes and vertical structure are in much better agreement with simulated data when applying the three-wavelength DIAL technique compared to using the two-wavelength technique. In the future, we will add new filters to obtain daytime NO_2 measurements. We also plan to purchase NO_2 balloonsondes for acquiring true validation data to evaluate HU lidar NO_2 results.

Code availability

The software code for this paper is available from the first author.

Data availability

The HU lidar data are archived at http://cas.hamptonu.edu/data-products/. DISCOVER-AQ data and WRF-Chem model output data are available from the first authors upon request.

Author contributions

JS designed the three-wavelength OPO DIAL system, did simulation works for the system, developed the NO_2 retrieval algorithm, and prepared the original manuscript. PMM was responsible for funding acquisition. MSJ provided simulated data from WRF-Chem model to verify NO_2 retrieval in this study. JTS, MJN, TAB, SK and GPG contributed to the analysis of NO_2 retrieval uncertainty. All listed authors contributed to the review and editing of this paper.

Competing interests

The authors declare that they have no conflict of interest.

Acknowledgments

We thank NASA TOLNet and NASA DISCOVER-AQ measurements for our simulation work. Matthew Johnson's contribution was supported by the NASA's TOLNet Science Team and the Tropospheric Composition Program. We also thank Dr. Gabriele Pfister from the Atmospheric Chemistry Observations & Modeling Lab at the National Center for Atmospheric Research for providing the WRF-Chem calculation applied in this study.

Financial support

This study was supported by the PIRT project funded by US Army Research, Development and Engineering Command (AQC) Center (DOD) under HU PIRT Award # 551150-211150) and the National Oceanic and Atmospheric Administration- Cooperative Science Center for Earth System and Sciences and Remote Sensing Technologies (NOAA-CESSRST) under the Cooperative Agreement Grant #: NA16SEC4810008. The statements contained within the manuscript/research article are not the opinions of the funding agency or the U.S. government, but reflect the author's opinions.

Review statement

This paper was reviewed by Dr. Piet Stammes (Editor) and one anonymous referee.

Supplementary Material

S.1 Two-wavelength DIAL retrieval equation

Table s.1. Extinction and backscatter of molecule and aerosol for wavelengths of λ_1 and λ_2.

wavelength	Molecular backscattering	Aerosol backscattering	Molecular extinction	Aerosol extinction
$\boldsymbol{\lambda_1}$	$\left(\frac{\lambda_1}{\lambda_2}\right)^{-4}\boldsymbol{\beta_m}$	$\left(\frac{\lambda_1}{\lambda_2}\right)^{-e}\boldsymbol{\beta_a}$	$\left(\frac{\lambda_1}{\lambda_2}\right)^{-4}\boldsymbol{\alpha_m}$	$\left(\frac{\lambda_1}{\lambda_2}\right)^{-e}\boldsymbol{\alpha_a}$
$\boldsymbol{\lambda_2}$	$\boldsymbol{\beta_m}$	$\boldsymbol{\beta_a}$	$\boldsymbol{\alpha_m}$	$\boldsymbol{\alpha_a}$

The two elastic lidar equations can be expressed as:

$$X(\lambda_1, Z) = C_1 \frac{\left[\left(\frac{\lambda_1}{\lambda_2}\right)^{-4}\beta_m(Z)+\left(\frac{\lambda_2}{\lambda_1}\right)^{-e}\beta_a(Z)\right]}{Z^2}\exp\left\{-2\int_0^Z\left[\left(\frac{\lambda_1}{\lambda_2}\right)^{-4}\alpha_m(z)+\left(\frac{\lambda_2}{\lambda_1}\right)^{-e}\alpha_a(z)+\sigma_N(\lambda_1,z)N_N(z)+O_{abs}(\lambda_1,z)\right]dz\right\} \quad \text{(s.1)}$$

$$X(\lambda_2, Z) = C_2 \frac{[\beta_m(Z)+\beta_a(Z)]}{Z^2}\exp\{-2\int_0^Z[\alpha_m(z)+\alpha_a(z)+\sigma_N(\lambda_2,z)N_N(z)+O_{abs}(\lambda_2,z)]dz\} \quad \text{(s.2)}$$

where X is the lidar signal; C_1 and C_2 are lidar constants; the subscripts a and m represent aerosol, and molecule, respectively; σ_N is the absorption cross section for the gas of interest; N_N is the molecular density of the gas of interest; O_{abs} is absorption of gases other than the gas of interest and z is the altitude. The molecular density of the gas of interest can be obtained after taking ratio of Eq. (1) to Eq. (2).

NO_2 density retrieval equation can be expressed as Eq. (3):

$$N_N(Z) = \frac{\frac{1}{2}\times\frac{d}{dz}\left[ln\frac{X(\lambda_1,Z)}{X(\lambda_2,Z)}\right]-AED(z)-MED(z)-OAD(z)-B(z)}{\Delta\sigma_N} \quad \text{(s.3)}$$

$$\Delta\sigma_N = \sigma_N(\lambda_2) - \sigma_N(\lambda_1) \quad \text{(s.4)}$$

$$B(z) = \frac{1}{2}\frac{d}{dz}\left[ln\frac{\left(\frac{\lambda_1}{\lambda_2}\right)^{-4}\beta_m(Z)+\left(\frac{\lambda_1}{\lambda_2}\right)^{-e}\beta_a(Z)}{\beta_m(Z)+\beta_a(Z)}\right] \quad \text{(s.5)}$$

$$AED(z) = \left[1-\left(\frac{\lambda_1}{\lambda_2}\right)^{-e}\right]\alpha_a(Z) \quad \text{(s.6)}$$

$$MED(z) = \left[1-\left(\frac{\lambda_1}{\lambda_2}\right)^{-4}\right]\alpha_m(Z) \quad \text{(s.7)}$$

$$OAD(z) = O_{abs}(\lambda_2, z) - O_{abs}(\lambda_1, z) \quad \text{(s.8)}$$

S.2 Units for all variables

Table s.2. Units for all variables

Items	Description	Unit
C1, C2,C3	lidar constant	constant (number)
α	extinction coefficient	km^{-1}
β	backscattering coefficient	$km^{-1}sr^{-1}$
λ	wavelength	nm
σ	absorption cross section	$cm^2molecule^{-1}$
Z, z	altitude	km
X	lidar range-corrected signal	mv
N	number density	$molecule/cm^3$

S	lidar ratio	sr^{-1}
U	Relative uncertainty	%

446

447 **Reference:**

448 Amnuaylojaroen T., Macatangay R.C., and Khodmanee S.: Modeling the effect of VOCs from
449 biomass burning emissions on ozone pollution in upper Southeast Asia, Heliyon., 5(10), e02661,
450 2019.

451 Barten, J. G. M., Ganzeveld, L. N., and Visser, A. J.: Rodrigo Jiménez, and Maarten C.Krol,
452 Evaluation of nitrogen oxides (NO_x) sources and sinks and ozone production in Colombia and
453 surrounding areas, Atmos. Chem. Phys., 20, 9441–9458, 2020.

454 Beirle, S., Boersma, K., Platt, U., Lawrence, M., and Wagner, T.: Megacity Emissions and
455 Lifetimes of Nitrogen Oxides Probed from Space, Science., 333, 1737–1739, 2011.

456 Beirle, S., Platt, U., Wenig, M., and Wagner, T.: Weekly cycle of NO_2 by GOME measurements:
457 a signature of anthropogenic sources, Atmos. Chem. Phys., 3(6), 2225–2232,2003.

458 Berg, N., Mellqvist, J., Jalkanen, J. P., and Balzani, J.: Ship emissions of SO_2 and NO_2: DOAS
459 measurements from airborne platforms, Atmos. Meas. Tech., 5(5), 1085–1098, 2012.

460 Berglund, M., Boström, C. E., Bylin, G., Ewetz, L., Gustafsson, L., Moldéus, P., Norberg, S.,
461 Pershagen, G., and Victorin, K.: Health risk evaluation of nitrogen oxides, Scandinavian journal
462 of work: environment and health., 19, 1993.

463 Bertram, T. H., Heckel, A., Richter, A., Burrows, J. P., and Cohen, R. C.: Satellite measurements
464 of daily variations in soil NO_x emissions, Geophys. Res. Lett., 32, L24812, 2005.

465 Boersma, K. F., Jacob, D. J., Eskes, H. J., Pinder, R. W., Wang, J., and Van Der A, R. J.:
466 Intercomparison of SCIAMACHY and OMI tropospheric NO_2 columns: Observing the diurnal
467 evolution of chemistry and emissions from space, J. Geophys. Res., 113, D16S26, 2008.

468 Bovensmann, H., Burrows, J. P., Buchwitz, M., Frerick, J., Noel, S., Rozanov, V. V., Chance, K.
469 V., and Goede, A. P. H.: SCIAMACHY: Mission objectives and measurement modes, J. Atmos.
470 Sci., 56(2), 127–150, 1999.

471 Bucsela, E. J., et al.: Comparison of tropospheric NO_2 in situ aircraft measurements with near-
472 real-time and standard product data from the Ozone Monitoring Instrument, J. Geophys. Res.,
473 113, D16S31, doi:10.1029/2007JD008838, 2008.

Celarier, E. A., et al.: Validation of Ozone Monitoring Instrument nitrogen dioxide columns, J. Geophys. Res., 113, D15S15, doi:10.1029/ 2007JD008908, 2008.

Chen, Y., Jie Wang, Huang, J., and Hu, Shunxing. (2017). Measurement of atmospheric NO_2 profile using three-wavelength dual-differential absorption lidar, Proc. SPIE., 10605, 106053L, 2017.

Cui, Y. Z., J. Lin, T., Song, C. Q., Liu, M. Y., Yan, Y. Y., Xu, Y., and Huang, B.: Rapid growth in nitrogen dioxide pollution over Western China 2005-2013, Atmos. Chem. Phys.,16(10), 2016.

Edward V. B., Syed I., and Scott T. S.: Ultraviolet DIAL measurements of O_3 profiles in regions of spatially inhomogeneous aerosols, Appl. Opt., 24, 2827-2836,1985.

Fernald, F. G., Herman, B. M., and Reagan, J. A.: Determination of aerosol height distributions by lidar, Journal of Applied Meteorology., 11(3), 482-489, 1972

Fredriksson, K. A. and Hertz, H. M.: Evaluation of the DIAL technique for studies on NO_2 using a mobile lidarsystem, Appl. Opt., 23(9), 1403–1411, 1984.

Georgoulias,A. K., Boersma, K. F., Vliet, J., Zhang, X., Ronald, A., Zani, P., and Laa, J.: Detection of NO2 pollution plumes from individual ships with the TROPOMI/S5P satellite sensor, Environ. Res. Lett., 15, 124037, 2020

Herman, J., Cede, A., Spinei, E., Mount, G., Tzortziou, M., and Abuhassan, N.: NO_2 column amounts from ground-based Pandora and DOAS spectrometers using the direct-sun DOAS technique: Intercomparisons and application to OMI validation, J. Geophys. Res., 114(D13), 2009.

Kollonige, D. E., Thompson, A. M., Josipovic, M., Tzortziou, M., Beukes, J. P., Burger, R., Martins, D. K., van Zyl, P. G., Vakkari, V., and Laakso, L.: OMI satellite and ground‐based Pandora observations and their application to surface NO2 estimations at terrestrial and marine sites, Journal of Geophysical Research., 123, 1441– 1459, 2018.

Kuang, S., M. J. Newchurch, J. Burris, and X. Liu (2013), Ground-based lidar for atmospheric boundary layer ozone measurements, Appl. Opt., 52, 3557-3566, http://dx.doi.org/10.1364/AO.52.003557.

Kuang, S., Wang, B., Newchurch, M. J., Knupp, K., Tucker, P., Eloranta, E. W., Garcia, J. P., Razenkov, I., Sullivan, J. T., Berkoff, T. A., Gronoff, G., Lei, L., Senff, C. J., Langford, A. O., Leblanc, T., and Natraj, V.: Evaluation of UV aerosol retrievals from an ozone lidar, Atmos. Meas. Tech., 13, 5277–5292, https://doi.org/10.5194/amt-13-5277-2020, 2020.

Lamsal, L. N., et al.: Evaluation of OMI operational standard NO_2 column retrievals using in situ and surface‐based NO_2 observations, Atmos. Chem. Phys., 14, 11,587–11,609, 2014.

Larkin, A., Geddes, J. A., Martin, R. V., Xiao, Q., Liu, Y., Marshall, J. D., Brauer, M., and Hystad, P.: Global Land Use Regression Model for Nitrogen Dioxide Air Pollution. Environmental Science and Technology., 51(12), 6957-6964, 2017.

Leblanc, T., Sica, R. J., van Gijsel, J. A. E., Godin-Beekmann, S., Haefele, A., Trickl, T., Payen, G., and Liberti, G.: Proposed standardized definitions for vertical resolution and uncertainty in the NDACC lidar ozone and temperature algorithms – Part 2: Ozone DIAL uncertainty budget, Atmos. Meas. Tech., 9, 4051–4078, https://doi.org/10.5194/amt-9-4051-2016, 2016.

Li, Z., Guo, J., Ding, A., Liao, H., Liu, J., Sun Y., Wang, T., Xue, H., Zhang, H., and Zhu, B.: Aerosol and boundary-layer interactions and impact on air quality, National Science Review., 4(6), 2017.

Liang, M., Guan, P., and Zheng, K.: Remote sensing of atmospheric NO_2 by employing the continuous-wave differential absorption lidar technique, Opt. Express., 25, A953-A962, 2017.

Liu, Q., Chen,Yafeng, J., Wang, J., Hu, S.:Measurement of atmospheric NO2 profile using three-wavelength dual-differential absorption lidar, Proc. SPIE., 10605, LIDAR Imaging Detection and Target Recognition, 106053L, 2017 https://doi.org/10.1117/12.2295725

Lorente, A. B., Boersma K. F., Eskes, H. J., Veefkind, J. P., Geffen, J. H. G. M., Zeeuw, M. B., Denier, H. A. C., Beirle, S., and Krol, M. C.: Quantification of nitrogen oxides emissions from build-up of pollution over Paris with TROPOMI, Sci Rep., 9, 20033, 2019, https://doi.org/10.1038/s41598-019-56428-5,

Measures, R. M.: Laser remote sensing: fundamentals and applications, Wiley, 510, 1984.

Newchurch, M. J., Ayoub, M. A., Oltmans, S., Johnson, B., and Schmidlin, F. J.: Vertical distribution of ozone at four sites in the United States, J. Geophys. Res., 108(D1), 4031, 2003.

Reid, J. S., Kuehn, R. E., Holz, R. E., Eloranta, E. W., Kaku,K. C., Kuang, S., Newchurch, M. J., Thompson, A. M., Trepte, C. R., Zhang, J., Atwood, S. A., Hand, J. L., Holben, B. N., Minnis, P., and Posselt, D. J.: Ground based high spectral resolution lidar observation of aerosol vertical distribution in the summertime Southeast United States, J. Geophys. Res. Atmos., 122(2), 2970-3004, 2017, doi:10.1002/2016JD025798.

Rothe, K. W., Brinkmann, U., and Walther, H.: Applications of tunable dye lasers to air pollution detection: measurements of atmospheric NO_2 concentrations by differential absorption, Appl. Phys., 3(2), 1974.

Russell, A. R., Valin, L. C., and Cohen, R. C.: Trends in OMI NO_2 observations over the United States: effects of emission control technology and the economic recession, Atmos. Chem, Phys., 12, 12197–12209, https://doi.org/10.5194/acp-12-12197- 2012, 2012.

Sasano, Y., Browell, E. V., and Ismail, S.: Error caused by using a constant extinction/ backscattering ratio in the lidar solution, Applied Optics, 24, 3929-3932,1985.

Schuster, G., Dubovik, O., and Holben, B. N.: Ångström exponent and bimodal aerosol size distributions, J. Geophys. Res., 111, D07207, 2006.

Scott, D. C., Herman, R. L., Webster, C. R., May, R. D., Flesch, G. J., and Moyer, E. J.: Airborne Laser Infrared Absorption Spectrometer (ALIAS-II) for in situ atmospheric measurements of N_2O, CH_4, CO, HCL, and NO_2 from balloon or remotely piloted aircraft platforms, Appl. Opt., 38, 4609-4622, 1999.

Sluis, W. W., Allaart, M. A. F., Piters, A. J. M., and Gast, L. F. L.: The development of a nitrogen dioxide sonde, Atmos. Meas. Tech., 3, 1753–1762, https://doi.org/10.5194/amt-3-1753-2010, 2010.

Sullivan, J., Rabenhorst, S. D., Dreessen, J., McGee, T. J., Delgado, R., Twigg, L., and Sumnicht, G.: Lidar observations revealing transport of O_3 in the presence of a nocturnal low-level jet: Regional implications for "next-day" pollution, Atmospheric Environment., 158, 160-171, 2017.

Sullivan, J., McGee, T. J., Sumnicht, G. K., Twigg, L. W., and Hoff, R. M.: A mobile differential absorption lidar to measure sub-hourly fluctuation of tropospheric ozone profiles in the Baltimore–Washington, D.C. region, Atmos. Meas. Tech., 7, 3529–3548, 2014.

Sunesson, J. A.: Differential absorption lidar system for routine monitoring of tropospheric ozone, Appl. Opt., 33(30), 7045-7058, 1994.

U.S. EPA 2016. Climate change indicators in the United States, 2016. Fourth edition. EPA 430-R-16-004.

U.S. EPA 2018. Data from the Air Pollutant Emission Trends Data website. Accessed 2018.

https://www.epa.gov/air-emissions-inventories/air-pollutant-emissions-trends-data.

563 Valks, P., Pinardi, G., Richter, A., Lambert, J. C., Hao, N., Loyola, D., Van Roozendael, M., and
564 Emmadi, S.: Operational total and tropospheric NO_2 column retrieval for GOME-2, Atmos.
565 Meas. Tech., 4(7), 1491–1514, 2011.

566 Volten, H., Brinksma, E. J., Berkhout, A. J. C., Hains, J., Bergwerff, J. B., Van der Hoff, G.
567 R., Apituley, A., Dirksen, R. J., Calabretta, J. S., and Swart, D. P. J.: NO_2 lidar profile
568 measurements for satellite interpretation and validation, Journal of Geophysical Research.,
569 114(24), 2009.

570 Wang, Z., Nakane, H., Hu, H., and Zhou J.: Three-wavelength dual differential absorption lidar
571 method for stratospheric ozone measurements in the presence of volcanic aerosols, Appl. Opt.,
572 36, 1245-1252, 1997.

573 Weibring, P., Smith, J. N., Edner, H., and Svanberg, S.: Development and testing of a frequency-
574 agile optical parametric oscillator system for differential absorption lidar, Review of Scientific
575 Instruments., 74, 4478, 2003.